PROPERTIES OF PYGMY DIPOLE STRENGTH FROM THEORETICAL PERSPECTIVE*

Nils Paar, Amandeep Kaur

Department of Physics, Faculty of Science, University of Zagreb
Bijenička c. 32, 10000 Zagreb, Croatia

Received 14 December 2024, accepted 12 February 2025,
published online 10 April 2025

The investigation of pygmy dipole strength (PDS) provides crucial insights into low-energy dipole excitations that occur in neutron-rich nuclei and are also predicted in proton-rich systems. These excitations represent a unique mode of soft excitation predominantly driven by complex interplay of transitions involving weakly-bound neutrons but also with some proton contributions. Over the past years, diverse theoretical approaches ranging from macroscopic models to the shell model and nuclear energy density functional (EDF) theories have been employed to explore the characteristics and fragmentation of PDS. These studies have uncovered its dependence on the neutron excess and relationships with the key nuclear properties such as the symmetry energy and neutron skin thickness. The advances in theoretical understanding of PDS provided valuable guidance for experimental studies of exotic nuclei. This paper reviews major theoretical findings on PDS, emphasizing their relevance to nuclear structure and their implications for astrophysical phenomena.

DOI:10.5506/APhysPolBSupp.18.2-A31

1. Introduction

Exploring nuclear excitations remains crucial to understanding the fundamental properties of matter in the universe. Among various nuclear excitations, the pygmy dipole strength, often denoted as pygmy dipole resonance (PDR), has attracted significant attention due to its connection to the low-energy dipole strength observed in neutron-rich nuclei and predicted in proton-rich systems [1–5]. The term pygmy dipole strength (PDS) refers to a portion of the dipole response, driven primarily by transitions of neutrons in the outermost orbitals. The study of PDS is crucial for understanding nuclear structure far from stability and astrophysical phenomena, in particular nucleosynthesis in explosive stellar environments. It also serves as a

* Presented at the 57$^{\mathrm{th}}$ Zakopane Conference on Nuclear Physics, *Extremes of the Nuclear Landscape*, Zakopane, Poland, 25 August–1 September, 2024.

probe for the symmetry energy, a critical component of the nuclear equation of state, and linking key observables such as neutron skin thickness to the behavior of neutron-rich matter [5, 6]. The PDS also provides constraints on the phase transition density and pressure at the inner edge separating the liquid core and the solid crust of a neutron star [7]. The PDS strength represents an important contribution to the overall dipole polarizability of the E1 response in nuclei, providing additional quantity that can be used to constrain the isovector channel of the effective nuclear interactions and the symmetry energy of the nuclear equation of state [8].

There is a remarkable diversity of theoretical approaches for studying PDS. Over the past two decades, a variety of theoretical frameworks have been developed and applied in analyses of the PDS. The macroscopic models such as the generalized Goldhaber–Teller and Steinwedel–Jensen models, describe pygmy dipole excitation as the oscillation of three incompressible fluids: the excess neutrons, which form the neutron skin, oscillate against an isospin-inert core resulting in a dipole excitation [5]. In addition, a broad spectrum of microscopic approaches is available, including the shell model, various models based on nuclear energy density functional theory (EDF), and other approaches, as outlined in the following list:

1. Hartree–Fock + Random Phase Approximation (RPA) with Skyrme interaction;
2. Hartree–Fock–Bogoliubov model + quasiparticle RPA (QRPA) based on Skyrme or Gogny interactions;
3. Time-dependent Hartree–Fock model;
4. Dirac–Hartree + Relativistic RPA;
5. Relativistic Hartree–Bogoliubov (RHB) model + relativistic QRPA;
6. Interacting Boson Model (IBM);
7. Configuration Interaction Shell Model (CISM);
8. Second RPA (SRPA) and Subtracted SRPA (SSRPA);
9. Quasiparticle phonon model (QPM);
10. Relativistic Quasi-particle Time Blocking Approximation (RQTBA);
11. Equation of Motion Phonon Method;

and others. A detailed list of references for the models mentioned above can be found in [5]. As listed above, several variants of non-relativistic and relativistic EDFs have been employed in derivation of self-consistent quasiparticle random phase approximation (QRPA) that in addition to the effective nuclear interaction rooted in the EDF also includes pairing correlations. In addition, further theoretical developments included couplings to complex configurations, *e.g.*, in the quasiparticle phonon model (QPM), multiphonon models, model using the quasiparticle time blocking approximation (QTBA), extended theory of finite Fermi systems (ETFFS), and equation of motion phonon method (EMPM). In this way, the insight into fragmenation of the PDS has been achieved, allowing more reliable comparison with the experimental data [9, 10].

At the QRPA level, the nature of the PDS has been explored through the calculation of the transition strengths and a more detailed analysis of the relevant two-quasiparticle contributions contributed to the discussions on the collective properties of the PDS. The studies of the isotopic and isotone dependence of the PDS allowed for additional insight into the dependence of the PDS transition strength and energy with the neutron excess. The covariance analysis in the EDF framework identified relevant correlations between the observables on the PDS and various properties of finite nuclei and nuclear matter. Of particular interest are correlations with the parameters of the symmetry energy, providing potential constraints for neutron-rich nuclear matter properties and neutron skin thickness in nuclei [11]. The comprehensive analyses underscore the importance of theoretical frameworks in revealing the complex nature of pygmy dipole strength. A variety of theoretical approaches to the PDS contribute to a deeper understanding of the underlying nuclear structure mechanisms and offer valuable insights for the experimental studies [9, 10].

In this paper, we present a brief overview of selected results on PDS derived from diverse microscopic frameworks, including various formulations of self-consistent Random Phase Approximation (RPA). These approaches incorporate relativistic energy density functionals and account for pairing correlations, enabling a detailed exploration of low-energy dipole excitations. Within these theoretical models, critical properties of PDS, such as transition strengths, fragmentation patterns, and isotopic dependencies, are systematically analyzed, providing profound insights into the underlying mechanisms of nuclear structure and dynamics.

2. Properties of pygmy dipole strength

The pygmy dipole strength (PDS) plays a critical role in enhancing neutron capture reaction cross sections, a key factor in shaping the r-process nucleosynthesis pathways responsible for the production of heavy elements. Investigating the PDS in neutron-rich nuclei is crucial for understanding its contribution to astrophysical phenomena. Neutron-rich isotopes exhibit a pronounced neutron skin, prompting questions about whether the excess neutrons participate in collective oscillations characteristic of the pygmy dipole resonance (PDR) or contribute to non-collective strength. The measurements of low-lying electric dipole (E1) strength in both stable nuclei (*e.g.*, ^{40}Ca and ^{208}Pb) and neutron-rich exotic nuclei such as ^{130}Sn and ^{132}Sn provide compelling evidence for a PDR structure near 10 MeV [12]. These resonances typically exhaust a few percent of the E1 energy-weighted sum rule, underscoring their relevance in both nuclear structure studies and nucleosynthesis modeling [12]. Theoretical studies, including shell-model and RPA-based calculations, suggest that while low-lying dipole strength in light nuclei arises from non-collective single-neutron excitations, medium-heavy and heavy neutron-rich nuclei exhibit more collective PDR states characterized by fragmented strength distributions, as confirmed by the Coulomb dissociation experiments in ^{130}Sn and ^{132}Sn [12].

Figure 1 illustrates the isovector dipole strength distribution in ^{132}Sn calculated by the relativistic RPA (RRPA), highlighting the ground-state density profiles and transition densities for states at 15.3 MeV (GDR) and 7.8 MeV (PDR). Using the DD-ME2 interaction, the calculations reveal distinct structural dynamics: the GDR displays characteristic isovector oscillations with the opposing proton and neutron phases, while the PDR shows a neutron-skin oscillation against the core, dominated by isoscalar dynamics in the interior and extended neutron transition densities. The PDR, calculated above the neutron separation energy (7.53 MeV), exhausts $\sim 2\%$ of the energy-weighted sum rule, with minimal proton contributions and significant neutron particle–hole (*ph*) configurations. Studies across isotopic chains (Ni, Sn, Pb) confirm that PDR peaks typically lie above the neutron

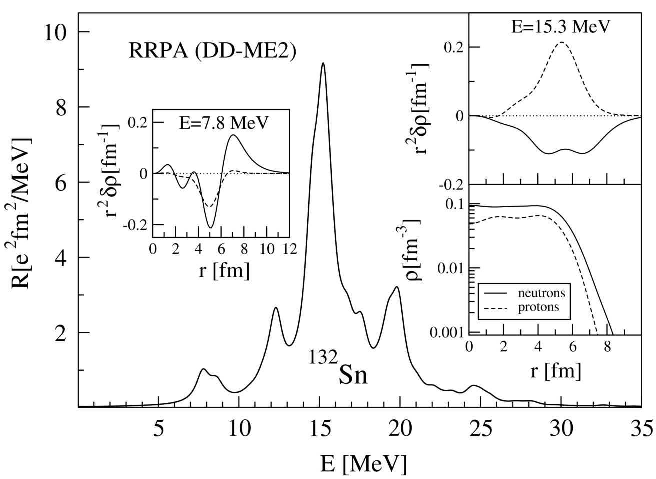

Fig. 1. The RRPA dipole strength distribution in ^{132}Sn, the ground-state density profiles of the neutron and proton distributions, and the neutron and proton transition densities for the GDR peak at 15.3 MeV, and the PDR peak at 7.8 MeV. Figure reprinted with permission from [1]. Copyright (2007) by the IOP.

emission threshold, aligning with experimental data, and remain robust even when particle-vibration coupling is considered, reinforcing the interpretation of the PDR as a resonant neutron-skin oscillation [13–15].

In order to compare the RQRPA and RQTBA methodologies based on the NL3* meson-exchange interaction and experimental low-energy electric dipole (E1) strength distributions on equal footing, the energy-weighted strength for the 4–10 MeV and 4–S_n ranges are shown in Fig. 2 for Sn isotopic chain [16]. Up to 10 MeV, the experimental strength exhausts $\sim 3\%–4\%$ of the TRK sum rule, including the IVGDR tail, while RQRPA and RQTBA predict a steady increase up to $\sim 7\%$ in ^{124}Sn. Both approaches concentrate strength near 8–10 MeV and predict more sub-threshold strength than experimental data, with the TRK values decreasing toward ^{124}Sn. The RQTBA shows improved but still imperfect agreement, suggesting missing mechanisms in the models.

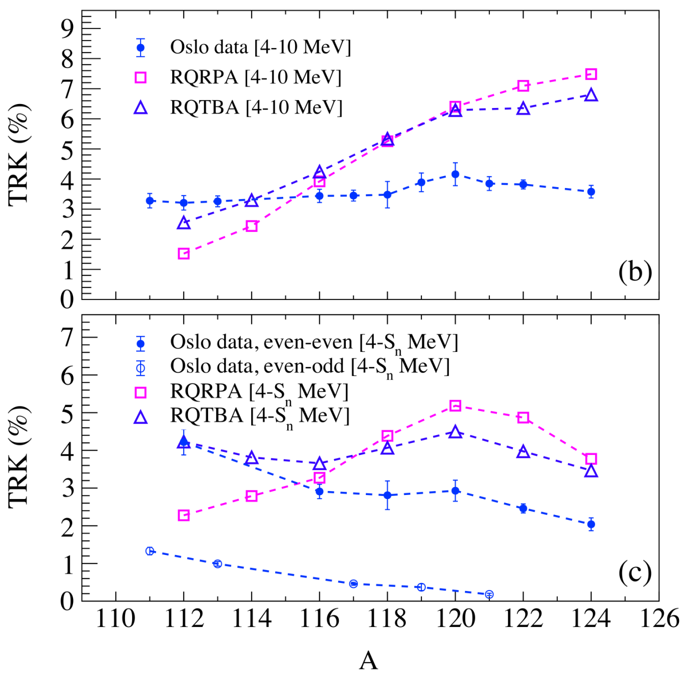

Fig. 2. The evolution of the energy-weighted electric dipole strength extracted from the RQRPA and RQTBA models based on the NL3* interaction, and the combined results of Oslo and $(p,\ p')$ measurements, integrated from 4 MeV up to (b) 10 MeV, and (c) neutron threshold S_n. Figure reprinted with permission from [16]. Copyright (2024) by the American Physical Society.

Moreover, Fig. 3 shows the evolution of energy-weighted PDS along the Sn isotopic chain, integrated up to cut-off energy $E_c = 10$ MeV, and plotted as a percentage of the classical TRK sum rule. These results are obtained within the RHB+RQRPA model by using relativistic DD-ME2 functionals with density-dependent vertex functions providing a realistic description of the symmetry energy [1]. The calculated low-lying E1 strength is in reasonable agreement with the experimental data for $^{116-124}$Sn and ^{130,132}Sn nuclei, rather different than the RQRPA and RQTBA results shown in Fig. 2 (b) that considerably overestimate the PDS energy-weighted strength. While the RQRPA and RQTBA calculations in Ref. [16] are based on the non-linear meson-exchange interaction NL3* with rather high value of the symmetry energy $J = 38.68$ MeV, the RQRPA calculation based on the density-dependent interaction DD-ME2 [1] provides a more realistic description of the isovector properties and symmetry energy $J = 32.3$ MeV, which are essential for the quantitative description of the PDS. In the first approximation, one could anticipate that, at least within a major shell, the relative strength of the PDR would rise monotonically with the number of neutrons when examining the evolution of low-lying dipole strength along an isotopic chain. A combination of shell effects and reduced pairing correlations leads to a reduction in the strength of the PDR in heavier Sn nuclei below $N = 82$. While the transition strength in the neighboring isotopes increases due to enhanced collectivity, or the increase in the number of two-quasiparticle pairs

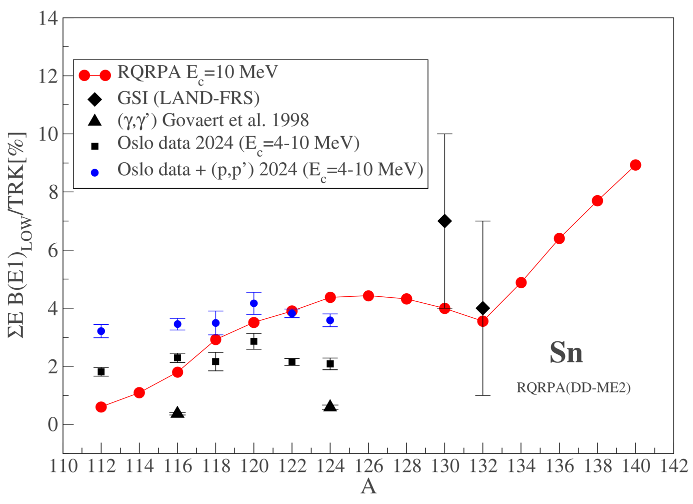

Fig. 3. The RHB + RQRPA energy-weighted dipole strength, integrated up to the energy cut-off $E_c = 10$ MeV, and plotted as a percentage of the TRK sum rule, along with experimental data. The calculation results from [1] are shown in comparison to new experimental Oslo data [16].

contributing to the RQRPA configuration space, the local minimum in the low-lying E1 strength is calculated for ^{132}Sn. In the neighboring isotopes, the transition strength increases due to enhanced collectivity, *i.e.* the increase in the number of two-quasiparticle pairs contributing to the RQRPA configuration space. We also observe a significant difference in the pygmy strength between exotic nuclei and nuclei near the valley of β-stability: the PDR strength shows a strong enhancement beyond ^{132}Sn, whereas below the $N = 82$ shell closure, the integrated transition strength is at most $\approx 4\%$ of the TRK sum rule value (for $E_{\mathrm{c}} = 10$ MeV).

To explore the nature of low-energy E1 transitions, the analysis of the contributions from individual particle–hole (ph) configurations to the total transition strength $B(\mathrm{E1})$ for the excited state of given energy has been carried out. Total E1 strength is calculated as $B(\mathrm{E1}) = |\sum_{ph} b_{ph}(\mathrm{E1})|^2$, and unperturbed excitation energy of ph pair is $E_{ph} = E_p - E_h$. Figure 4 depicts the partial contributions from the individual ph contributions (b_{ph}) [1] to the overall isovector transition strength of the pygmy state of ^{132}Sn at 7.74 MeV. The red/gray and blue/black bars indicate the partial contributions from protons and neutrons, respectively. Some degree of coherence in neutron transitions is observed, though partial cancellation of the transition strength also occurs. Below $E_{ph} < 10$ MeV, a coherent contribution from neutron transitions leads to a steady buildup of strength, which remains nearly constant at higher energies. However, the specific transitions responsible for these cancellations cannot be uniquely identified based solely on the information in Fig. 4. The analyses of PDS strengths and their single-

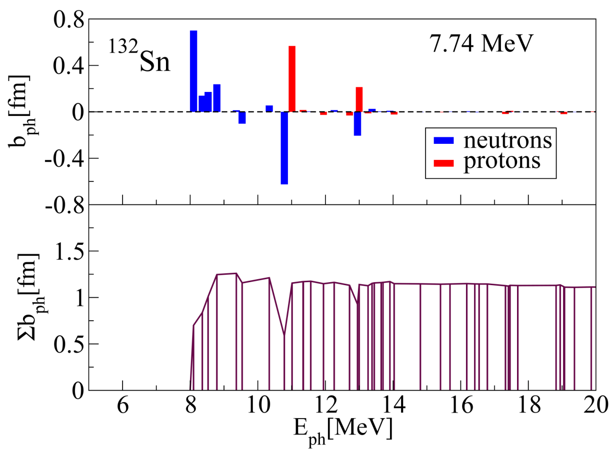

Fig. 4. (Color online) The upper panel shows the individual ph contributions to the overall isovector dipole strength for the PDS state at excitation energy 7.74 MeV for ^{132}Sn. The lower panel displays the running sum of the corresponding transition strength as the energy of ph pairs increases. Figure reprinted from [17].

particle composition indicated that their structure may be rather complex, containing both isoscalar and isovector components, as predicted by theoretical studies [18–21] and analyzed by experiment [22–27]. More details about experimental perspectives on low-energy dipole strength are also given in reviews [3, 9] and in Zilges [27, 28], Spieker [24, 25], Markova [16], and others.

A self-consistent microscopic approach incorporating quasiparticle–vibration coupling (qPVC) via $2q \otimes$ phonon configurations has been applied to study the dipole response of medium-mass ^{124}Sn nucleus [16]. This method, based on the leading role of $2q \otimes$ phonon configurations and the time-blocking technique, is referred to as the relativistic quasiparticle time-blocking approximation (RQTBA). Strength distributions obtained with RQTBA are compared to those obtained from RQRPA and experimental data, as shown in Fig. 5, using the NL3* meson-exchange interaction and a smearing parameter of $\Delta = 200$ keV. The inclusion of $2q \otimes$ phonon configurations in RQTBA significantly modifies the strength distribution, introducing fragmentation and shifting the strength to lower transition energies. Notably, the PDS region below 10 MeV exhibits significant structural differences between the RQTBA and RQRPA, with the IVGDR spreading and PDS fine structure largely arising from these configurations. This addition improves the description of experimental data, particularly the IVGDR width and the PDS fine structure.

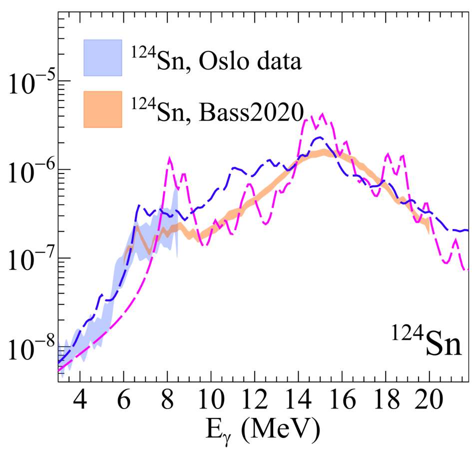

Fig. 5. (Color online) RQTBA and RQRPA calculated E1 strength for ^{124}Sn using the NL3* meson-exchange interaction. The blue/dark gray and orange/gray bands show the corresponding Oslo and (p, p') data. Figure reprinted with permission from [16]. Copyright (2024) by the American Physical Society.

The isovector dipole transition-strength distributions are sensitive to the properties of symmetry energy [11], as shown for ^{132}Sn in Fig. 6 [17]. These distributions were obtained using a set of DD-ME effective interactions that span the values of symmetry energy at saturation density, $J = 30$–38 MeV (and correspondingly the slope parameter $L = 30$–110.8 MeV). It is clear that J and L have a sensitive effect on the transition spectra. As J increases, the GDR's peak energy systematically shifts to lower values, and there is also some sensitivity in the transition strength. The PDS strength exhibits strong sensitivity to J as one can observe in the low-energy region, meaning that the transition strength significantly rises with J (by a factor ≈ 3–4). That means the PDS is strongly sensitive to the symmetry energy, and the studies of the PDS require effective interactions with reasonable values of J and L, such as density-dependent meson exchange or point coupling interactions, as demonstrated in Fig. 3.

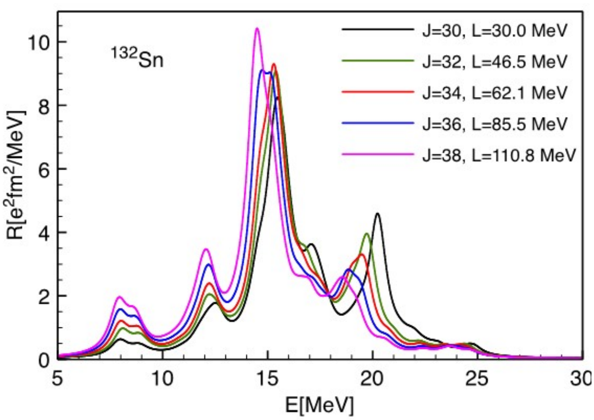

Fig. 6. Isovector E1 strength for ^{132}Sn for the set of density-dependent effective interactions spanning the range of values $J = 30$ to 38 MeV, and the corresponding L as denoted in the legend. Figure reprinted from [17].

Finally, it is to be noted that proton PDS in proton-rich nuclei was predicted theoretically almost two decades ago but has not yet been experimentally verified. For instance, Fig. 7 is an example of particularly pronounced proton PDS in proton-rich Ar isotopes [29] and shows the distribution of the RHB+RQRPA electric dipole strength in ^{32}Ar. There are prominent proton PDR peaks just below 10 MeV in addition to the rather fragmented GDR structure at 20 MeV. The mass dependence of the centroid energy of the pygmy peaks and the associated values of the integrated B(E1) strength below 10 MeV excitation energy are also shown in Fig. 7. The mass dependence of the PDR excitation energy and B(E1) strength in proton-rich isotopes is opposite to that of the GDR, in contrast to the case of medium-heavy and heavy neutron-rich isotopes, where both the PDR and GDR decrease in energy as the neutron number increases. As the proton excess increases, the proton PDRs energy decreases. Since we have demonstrated that transitions from the weakly-bound proton orbitals dominate the proton PDR mode, this mass dependence is expected. As one moves closer to the drip line, the number of $2qp$ configurations with weakly-bound proton orbitals rises, resulting in an enhancement of the low-lying B(E1) strength.

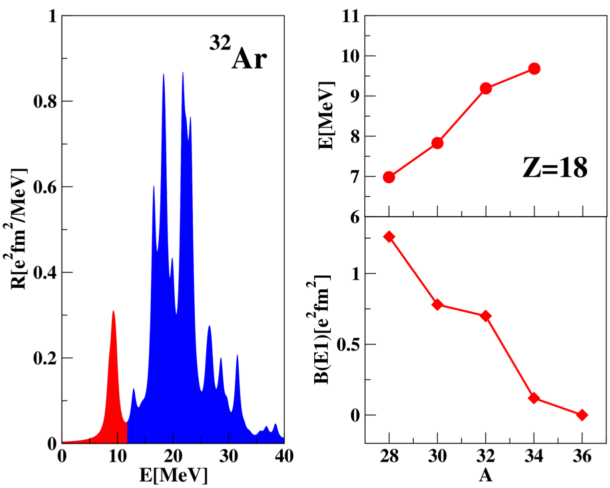

Fig. 7. The RHB+RQRPA isovector dipole strength distribution for ^{32}Ar (left panel). The right panel displays the mass dependence of the pygmy peak's centroid energy for the argon isotopes, with the integrated B(E1) strength below energy $E = 10$ MeV. Figure reprinted with permission from [29]. Copyright (2024) by the American Physical Society.

3. Conclusions

This work briefly reviews the properties of pygmy dipole strength from theoretical perspective. It provides an overview of various theoretical frameworks to analyze the structure of PDS, including transition strengths, fragmentation patterns, and isotopic dependencies. The findings underscore the importance of the PDS in exploring critical nuclear properties such as symmetry energy, neutron skin thickness, and overall nuclear structure. By demonstrating the sensitivity of PDS features to properties such as the neutron excess and symmetry energy, this overview offers valuable insights for experimental studies and enhances our understanding of exotic nuclei.

This contribution is supported by the Croatian Science Foundation under the project Relativistic Nuclear Many-Body Theory in the Multimessenger Observation Era (IP-2022-10-7773).

REFERENCES

[1] N. Paar, D. Vretenar, E. Khan, G. Colò, *Rep. Prog. Phys.* **70**, R02 (2007).

[2] T. Aumann, T. Nakamura, *Phys. Scr.* **T152**, 014012 (2013).

[3] D. Savran, T. Aumann, A. Zilges, *Prog. Part. Nucl. Phys.* **70**, 210 (2013).

[4] A. Bracco, F.C.L. Crespi, E.G. Lanza, *Eur. Phys. J. A* **51**, 1 (2015).

[5] E.G. Lanza *et al.*, *Prog. Part. Nucl. Phys.* **129**, 104006 (2023).

[6] C.A. Bertulani, *Eur. Phys. J. A* **55**, 240 (2019).

[7] N. Paar *et al.*, *Phys. Rev. C* **90**, 011304 (2014).

[8] E. Yüksel, N. Paar, *Phys. Lett. B* **836**, 137622 (2023).

[9] A. Bracco, E.G. Lanza, A. Tamii, *Prog. Part. Nucl. Phys.* **106**, 360 (2019).

[10] T. Aumann, *Eur. Phys. J. A* **55**, 234 (2019).

[11] X. Roca-Maza, N. Paar, *Prog. Part. Nucl. Phys.* **101**, 96 (2018).

[12] P. Adrich *et al.*, *Phys. Rev. Lett.* **95**, 132501 (2005).

[13] N. Paar, T. Nikšić, D. Vretenar, P. Ring, *Phys. Lett. B* **606**, 288 (2005).

[14] N. Ryezayeva *et al.*, *Phys. Rev. Lett.* **89**, 272502 (2002).

[15] E. Litvinova, P. Ring, D. Vretenar, *Phys. Lett. B* **647**, 111 (2007).

[16] M. Markova *et al.*, *Phys. Rev. C* **109**, 054311 (2024).

[17] N. Paar, A. Horvat, *EPJ Web Conf.* **66**, 02078 (2014).

[18] N. Paar, Y.F. Niu, D. Vretenar, J. Meng, *Phys. Rev. Lett.* **103**, 032502 (2009).

[19] D. Vretenar *et al.*, *Phys. Rev. C* **85**, 044317 (2012).

[20] E.G. Lanza, A. Vitturi, E. Litvinova, D. Savran, *Phys. Rev. C* **89**, 041601 (2014).

[21] I. Hamamoto, H. Sagawa, *Phys. Rev. C* **96**, 064312 (2017).

[22] J. Endres *et al.*, *Phys. Rev. Lett.* **105**, 212503 (2010).

[23] M. Krzysiek *et al.*, *Phys. Rev. C* **93**, 044330 (2016).

[24] M. Spieker *et al.*, *Phys. Rev. Lett.* **125**, 102503 (2020).

[25] M. Spieker *et al.*, *Phys. Rev. C* **108**, 014311 (2023).

[26] M. Weinert *et al.*, *Phys. Rev. Lett.* **127**, 242501 (2021).

[27] A. Zilges, D. Savran, «Pygmy Dipole Resonance: Experimental Studies by Different Probes», *Springer Nature*, Singapore 2020, pp. 1–28.

[28] M. Müscher *et al.*, *Phys. Rev. C* **109**, 044318 (2024).

[29] N. Paar, D. Vretenar, P. Ring, *Phys. Rev. Lett.* **94**, 182501 (2005).